www.czasopisma.pan.pl PAN POLSKA AKADEMIA NAUK www.journals.pan.pl

Arch. Metall. Mater. **62** (2017), 2B, 1057-1062

DOI: 10.1515/amm-2017-0153

S.H. CHOI*,**, B. ALI*,***, S.K. HYUN**, J.J. SIM*,**, W.J. CHOI*, W. JOO*,
J.H. LIM*, Y.J. LEE****, T.S. KIM*,***#, K.T. PARK*#

FABRICATION OF A SPHERICAL TITANIUM POWDER BY COMBINED COMBUSTION SYNTHESIS AND DC PLASMA TREATMENT

Combustion synthesis is capable of producing many types of refractory and ceramic materials, as well as metals, with a relatively lower cost and shorter time frame than other solid state synthetic techniques. TiO_2 with Mg as reductant were dry mixed and hand compacted into a 60 mm diameter mold and then combusted under an Ar atmosphere. Depending on the reaction parameters (Mg concentration $2 \leq \alpha \leq 4$), the thermocouples registered temperatures between 1160°C and 1710°C . 3 mol of Mg gave the optimum results with combustion temperature (T_c) and combustion velocity (U_c) values of 1372°C and 0.26 cm/s respectively. Furthermore, this ratio also had the lowest oxygen concentration in this study (0.8 wt%). After combustion, DC plasma treatment was carried out to spheroidize the Ti powder for use in 3D printing. The characterization of the final product was performed using X-ray diffraction, scanning electron microscopy, energy dispersive spectroscopy, and N/O analysis.

Keywords: Combustion synthesis, DC plasma treatment, Titanium powder, 3D printing process, Combustion parameters

1. Introduction

Titanium metal sees significant use in the aerospace, chemical processing, automotive and biomedical industries [1-2] due to its high strength to weight ratio, ductility, corrosion resistance and biocompatibility [3-4]. Recently, three-dimensional (3D) metal printing processes have been recognized as a flexible and rapid means of fabricating complex shapes such as implants and scaffolds, which are otherwise difficult to produce using conventional material processing techniques [5-9]. When Ti powder is used for 3D printing, it is best to use a spherical powder of approximately 100 μm diameter, in addition to having good powder flow, a tap density >65%, and low oxide content [11].

Commercial production of titanium is typically carried out using the Kroll process, which reduces titanium chloride to titanium metal [10]. The process involves three steps as shown in Fig. 1. The first step involves a chlorination process in which titanium oxide ore is converted to its chloride form. The second stage is based on the magnesiothermic reduction of titanium chloride and production of a titanium metal sponge. Lastly, the titanium sponge is converted into a powder through various gas atomization powder production techniques such as plasma rotating atomization, electrode induction melting gas atomization, and plasma wire atomization [11].

Despite numerous advancements in the Kroll process, such as producing clean Ti metal with higher than 3N purity and large-scale bulk materials (>1 ton/batch), it still requires multiple phase transitions (oxide → halide → metal), Cl_2 gas needed for preparing $TiCl_4$, long operation times, and a particularly costly raw material in Ti [12-13]. In addition, Ti sponge is used as a raw material in atomization processes for producing Ti powders, which involves re-melting and applying high pressure gas jets to a Ti melt. Owing to this fact, many researchers have sought an alternative to the Kroll process, such as the Hunter, Fray-Farthing-Chen, and Ono-Suzuki processes [14-16].

Self-propagating high temperature synthesis (SHS) and simple combustion synthesis (CS) have been studied for the fabrication of Ti powder [17-18]. CS is a highly sophisticated and efficient powder production technique that has many advantages over other conventional processes, such as fast production rate, high energy efficiency, direct oxide reduction, simplified equipment and high purity in the final products (Fig. 1) [19].

In this study, the possibility of directly reducing TiO_2 to Ti metal by CS is investigated. TiO_2 is used as the raw material, while Mg metal is utilized as a reducing agent. The molar ratio of Mg is controlled as a process parameter of Ti powder preparation. After CS, DC plasma treatment is carried out to spheroidize the Ti powder into a raw material for 3D printing.

* KOREA INSTITUTE FOR RARE METALS, KOREA INSTITUTE OF INDUSTRIAL TECHNOLOGY, ELEVENTH FLOOR, GET-PEARL TOWER, GAETBEOL-RO 12, YEONSU-GU, INCHEON, SOUTH KOREA
** DEPARTMENT OF ADVANCED MATERIALS ENGINEERING, IN-HA UNIVERSITY, IN-CHEON, SOUTH KOREA
*** DEPARTMENT OF RARE METALS ENGINEERING, UNIVERSITY OF SCIENCE AND TECHNOLOGY, DAE-JEON, SOUTH KOREA
**** DEPARTMENT OF ADVANCE MATERIAL ENGINEERING, CHUNGNAM NATIONAL UNIVERSITY, DAEJEON, SOUTH KOREA

Corresponding authors: ktpark@kitech.re.kr and tskim@kitech.re.kr

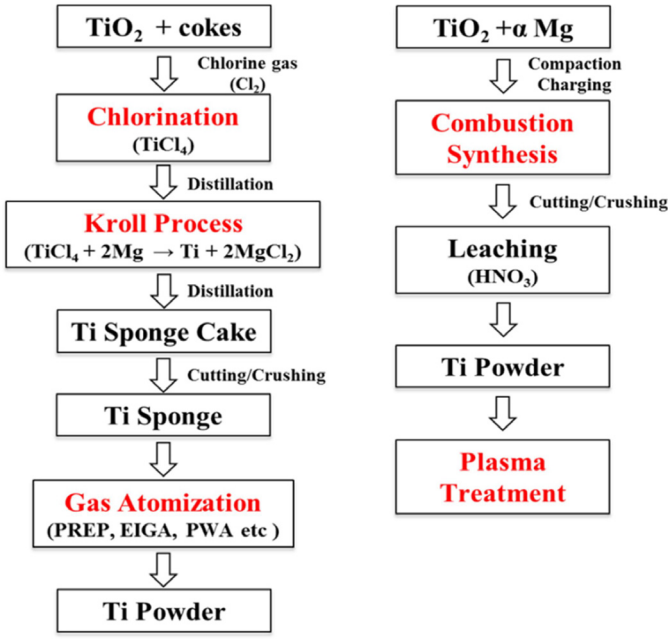

Fig. 1. Flow charts of (a) conventional Ti powder manufacturing and (b) the CS process

2. Experimental

2.1. Preparations of Combustion Synthesis and Spheroidization

Titanium dioxide powder (TiO_2, 99.99%, particle size 2 μm, Kojundo Chemical Laboratory Co., Ltd, Japan) and magnesium powder (Mg, >98.5%, particle size <74 μm, DaeJung Chemicals & Metals Co., Ltd, S. Korea) were used as raw materials. These materials in molar ratios of 1:2 to 1:4 (TiO_2:Mg) were dry mixed for 30-60 min using a mortar, and then hand compacted in a cylindrical mold 60 mm in diameter and 120 mm high. This mixture was then placed in a steel autoclave with under Ar gas (2.5 MPa) and ignited with a resistively heated Nichrome (Ni-Cr) wire.

During combustion, the synthesis follows the chemical pathway shown in Eq. 1. The combustion temperature (T_c) was measured by inserting W-Re Type-C thermocouples (W-Re 26%/W-Re 5%) in the middle and bottom of the sample. These thermocouples were coated with ceramic material in order to prevent any reaction with the mixture powder. Time, temperature and pressure profiles were continuously recorded at a time interval of 0.1 s. From these data, the combustion wave propagation velocity (U_c) was calculated as $U_c = x/t$ (x: distance between thermocouples, t: time interval between temperature profiles).

The obtained burnt sample was loosely sintered. The surface layer was partially removed and the sample was ground into a powder. In order to remove the Mg and MgO byproducts predicted by Eq. 2, this powder was treated with dilute nitric acid (HNO_3, DukSan PureChemicals Co., Ltd, 64-66%) by stirring the mixture for 1.5 h and subsequently rinsing it with distilled water. The mixture was then dried at 80°C for 24 h to obtain the final Ti powder. Spheroidization and size control of the Ti powder was carried out using DC plasma treatment, using the parameters shown in Table 1.

TABLE 1

Experimental conditions of DC plasma treatment

Classification	Power (kW)	Current (A)	Voltage (V)	Discharge Gas (L/min)	Pressure (torr)	Feeding rate	Carrier gas (L/min)
Parameter	9.0	300	30	Ar, 15	760	1.0 g/min	Ar, 3

$$TiO_2 + \alpha\,Mg \rightarrow Ti + 2MgO + (\alpha - 2)\,Mg \quad (1)$$

$$Ti + MgO\,(Mg) + 2HNO_3 + nH_2O \rightarrow Ti + Mg\,(NO_3)_2 + (n+1)\,H_2O \quad (2)$$

2.2. Analysis of combustion products

Thermodynamic calculations (equilibrium concentration of the reaction phases (mole) and adiabatic combustion temperature T_{ad} (°C)) were performed using the FactSage 7.0 software, equilibrium module (CRCT-Thermfact Inc., Canada & GTT-Technologies, Germany). Adiabatic temperature (T_{ad}) was calculated using Eq. 3.

$$-\Delta H_f^0(T_0) = \int_{T_0}^{T_m} C_{Ps}(P)\,dT + \Delta H_m + \int_{T_m}^{T_{ad}} C_{Pl}(P)\,dT, \text{ if } T_{ad} > T_m \quad (3)$$

Phase identification of the combusted powder was performed using X-ray diffraction (XRD, Rigaku RINT-TTR, Japan). The powder morphology was analyzed by field emission scanning electron microscopy (FE-SEM, JEOL JSM-7100F, Japan) and the particle size distribution was calculated using dry particle size analysis (PSA, Beckman Coulter LS I3 320, USA). The oxygen content of powder was estimated by N/O analysis (Eltra GmbH ONH 2000, Germany). Activation energy of the $TiO_2 + \alpha Mg$ (where α = molar concentration of Mg) system was calculated from an Arrhenius plot drawn by utilizing U_c and T_c values. An experimental flow diagram of this study is presented in Fig. 2.

3. Results and discussion

CS utilizes an exothermic heat of reaction for synthesis. Therefore, the first step in designing a CS reaction is to choose a combination of reactive elements that reacts in an exothermic manner. Generally, a combination of a metal oxide and a reducing element such as Mg or Al is used, where exothermic heat is

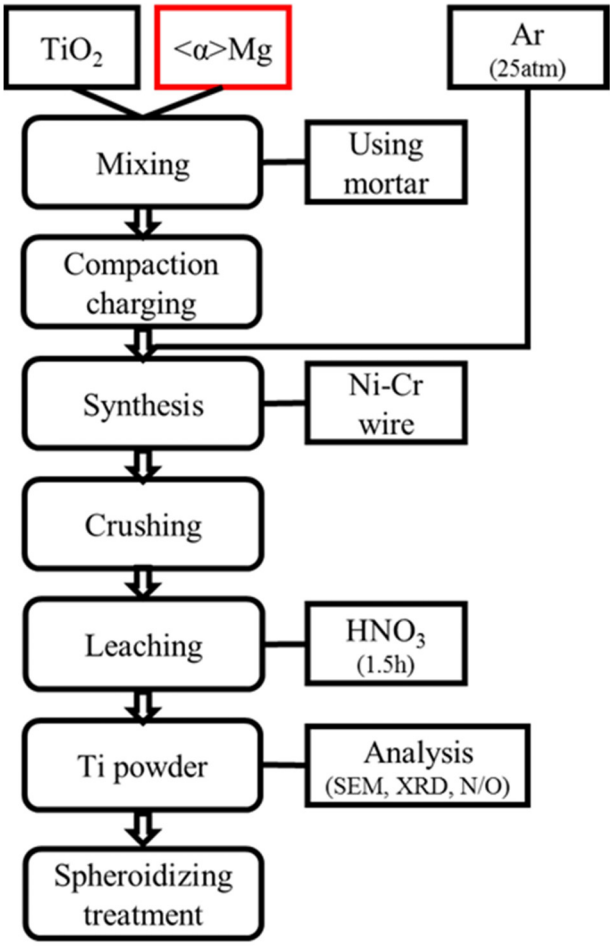

Fig. 2. Experimental Process flow diagram

generated during the reduction of the metal oxide to pure metal. The general form of this process is shown in Eq. 4.

$$\text{MeO (Metal Oxide)} + \text{Re (Reducing Agent)} \rightarrow \text{Me} + \text{ReO} + \text{Q} \quad (4)$$

Based on the above, Mg metal powder was chosen for the reduction of titanium oxide to titanium.

3.1. Thermodynamic analysis

Prior to these experiments, thermodynamic calculations for adiabatic combustion temperature (T_{ad}) and equilibrium composition of the reaction products of the TiO_2 + αMg system were carried out using the FactSage software (Fig. 3).

T_{ad} decreases as the Mg molar ratio increases, and the maximum value of T_{ad} (1805°C) is expected at a stoichiometric point of α = 2, where the system consists of only Ti and MgO phases. Below this stoichiometric point, T_{ad} decreases slightly due to evaporation of Mg as the reaction temperature increases; here the system is expected to be mainly composed of Ti, TiO and MgO. At $\alpha > 2$, T_{ad} continues to decrease due to excess Mg, as the melting of excess Mg causes the reaction to become more endothermic. Here, the reaction products are Ti, MgO and Mg.

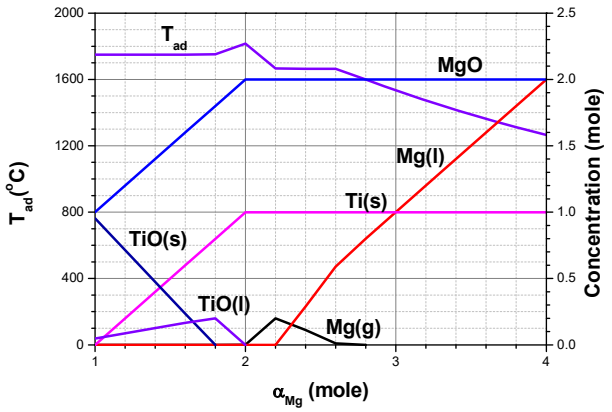

Fig. 3. Thermodynamic calculation of adiabatic combustion temperature and equilibrium phase concentration in the TiO_2 + αMg system

3.2. Characteristics of combustion products

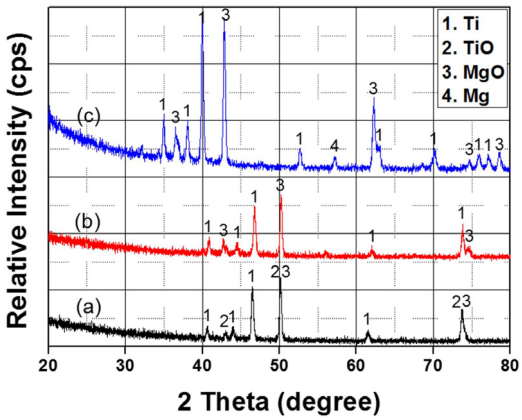

Fig. 4. XRD results of titanium powder: (a) α = 2, (b) α = 3, (c) α = 4, before leaching

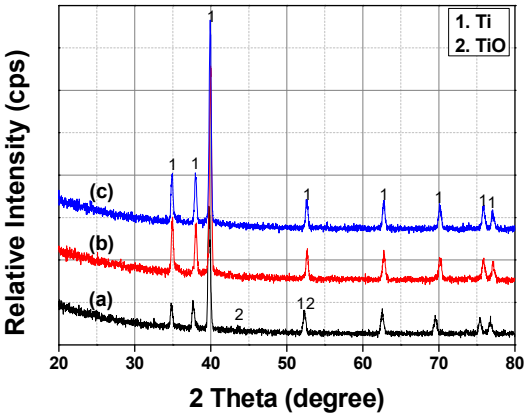

Fig. 5. XRD results of combustion products: (a) α = 2, (b) α = 3, (c) α = 4, after leaching

Fig. 4 and Fig. 5 show XRD results for the TiO_2 + αMg system ($2 \leq \alpha \leq 4$) before and after acid leaching, respectively. Before leaching (Fig. 4a)), the combustion product consists of reduced Ti, MgO and an intermediate TiO phase (α = 2), where this TiO phase is present because of the high combustion temperature. At high reaction temperatures, Mg is melted and

vaporized by the exothermic heat in the adiabatic chamber. At $\alpha = 2$, Mg is not efficiently used for reduction which leads to intermediate oxides like TiO to be present in the system. This allows Mg vapor to leave the mixture, leading to an inefficient conversion of TiO_2 into Ti. This effect can be minimized by adding excess Mg (Fig. 4b,c), which minimizes the TiO phase. However, at $\alpha = 4$ (Fig. 4c)), unreacted Mg is also present. After leaching (Fig. 5), MgO and residual Mg were removed and Ti peaks are present for all conditions, indicating successful oxide reduction. However, a small amount of TiO is observed for $\alpha = 2$.

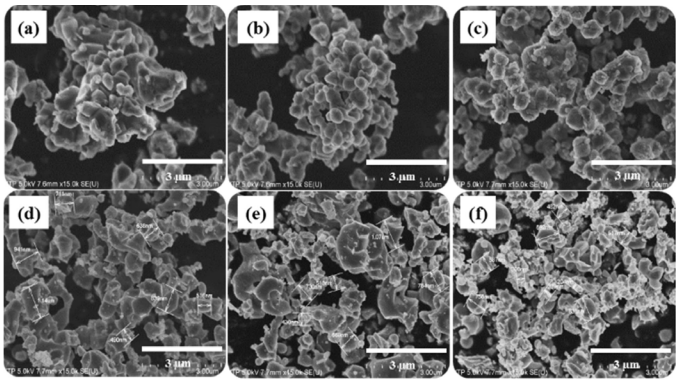

Fig. 6. FE-SEM images of the Ti powders: (a-c) before leaching, (d-f) after leaching

SEM analysis of the as-synthesized powder was also performed. Fig. 6 shows FE-SEM images of Ti particles before leaching (a-c) and after leaching (d-f), prepared at $\alpha = 2$, 3, and 4. Before leaching, large agglomerated particles were present, whereas after leaching these particles became more dispersed. The overall size of the Ti particles clearly decreased as the molar ratio of Mg increased. As the Mg concentration increased, the combustion and reaction temperatures decreased, while the reaction time increased. This causes molten Mg to remain in contact with TiO_2 for a longer period of time. As a result, an MgO layer is formed around the reduced Ti particle, which stops further grain growth and limits contact between adjacent Ti particles.

The oxygen concentration of the Ti powder was also measured, the results of which are shown in Fig. 7.

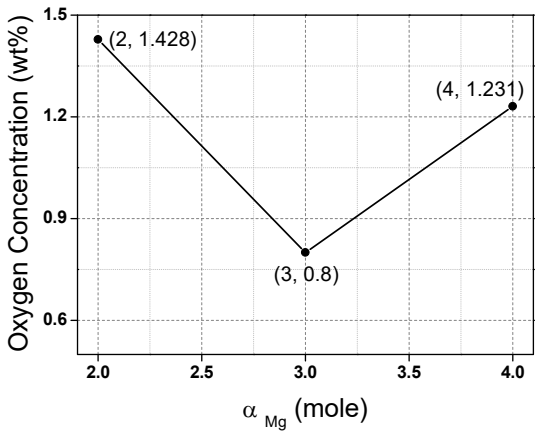

Fig. 7. Oxygen concentration of Ti powder obtained from the $TiO_2 + \alpha$Mg system

A lowest oxygen concentration of 0.8 wt% was present at $\alpha = 3$, while the highest value (1.428 wt%) occurred at $\alpha = 2$ because of the incomplete reduction of TiO_2.

3.3. Combustion parameters

Fig. 8 shows the effects of varying the Mg concentration on the combustion temperature (T_c) and combustion wave propagation velocity (U_c) of this system.

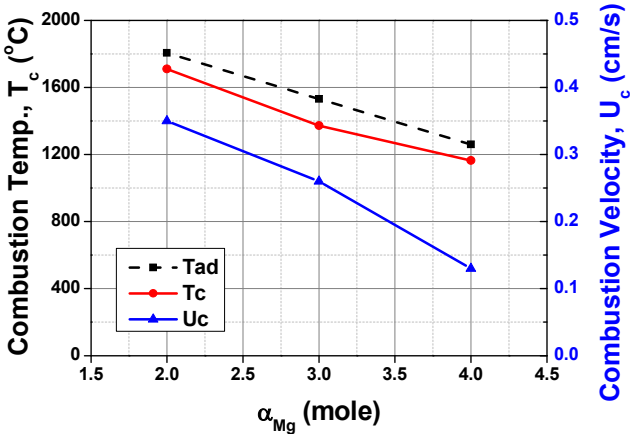

Fig. 8. Combustion parameters of the $TiO_2 + \alpha$Mg system

T_{ad} and T_c differ from each other because the reaction cannot be run under perfectly adiabatic conditions. As predicted by our thermodynamic calculations (Fig. 3), T_c and U_c decrease as the Mg concentration increases. The lowest values of T_c (1164°C) and U_c (0.13 cm/s) were calculated for $\alpha = 4$, while the highest T_c (1709°C) and U_c (0.35 cm/s) were obtained at $\alpha = 2$. This change in U_c and T_c can be explained by the changes in the thermal conductivity of combustion zone as the Mg concentration changes, as it greatly influences the density and size of the initial mixture. As mentioned in section 3.2, $\alpha = 3$ yields optimum oxygen conditions for the $TiO_2 + \alpha$Mg system ($2 \leq \alpha \leq 4$).

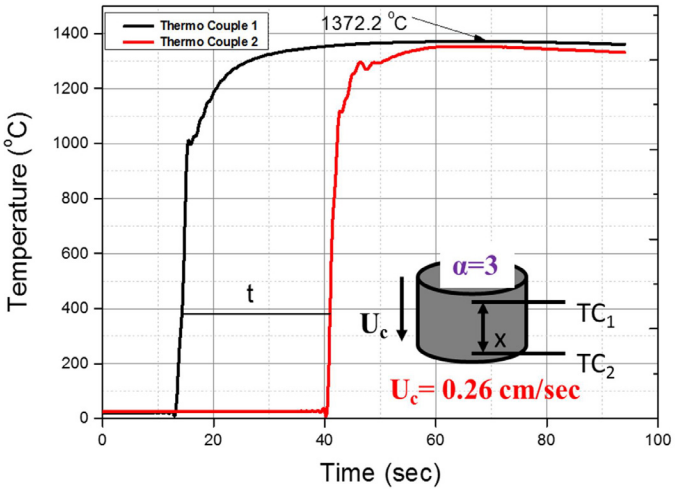

Fig. 9. Temperature-time profile recorded during the combustion of the $TiO_2 + \alpha$Mg system

The time-temperature profile for the $\alpha = 3$ system is shown in Fig. 9, where the obtained T_c and U_c values are 1372.2°C and 0.26 cm/s respectively.

By utilizing changes in U_c and T_c based on changes to the Mg concentration, the activation energy of the TiO_2 + αMg system can be calculated using Eqs. 5-7.

$$U_c^2 = AT_c \exp\left(-\frac{E}{RT_c}\right) \tag{5}$$

$$\ln\left(\frac{Uc}{T_c}\right) = -\frac{E}{2RT_c} + \ln A \tag{6}$$

$$\ln\left(\frac{Uc}{T_c}\right) = -\frac{E}{2R}\cdot\frac{1}{T_c} + \ln A \tag{7}$$

As ln (U_c/T_c) depends linearly on $(1/T_c)$ [20], Fig. 10 plots ln (U_c/T_c) and $(1/T_c)$, indicating that the activation energy of the TiO_2 + αMg ($2 \le \alpha \le 4$) system is 20.5 kJ/mol.

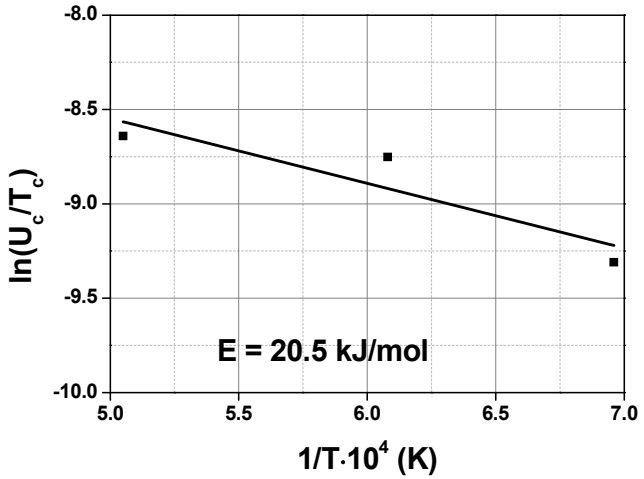

Fig. 10. Arrhenius plot [lnU_c/T_c vs $1/T_c$] for the combustion of the TiO_2+αMg system

This value is low because Mg is in liquid state before the reaction, while TiO_2 is still solid. The liquid Mg begins to diffuse into the solid TiO_2 phase, which lowers the activation energy required to carry out the reaction. Combustion parameters for the reaction mixture are summarized in Table 2.

TABLE 2

Combustion parameters of the TiO_2 + αMg system

Mg concentration (mole)	Adiabatic Temp. (T_{ad})	Combustion Temp. (T_c)	Combustion Velocity (U_c)	Green Density	Activation energy
2	1815.53	1709	0.35 cm/sec	0.935 g/cm^3	20.5 kJ/mol
3	1534.27	1372.2	0.26 cm/sec	1.324 g/cm^3	
4	1264.8	1164	0.13 cm/sec	1.376 g/cm^3	

3.4. DC Plasma Treatment

As shown in Fig. 6, the CS process tends to yield irregular particle shapes, while spherical particles are more desirable for metal 3D printing. Spheroidization was carried out on the as-synthesized Ti powder using DC plasma treatment, which is a sophisticated technique for controlling powder purity and size. Fig. 11 shows Ti powder morphology and size distributions before and after plasma treatment. After spheroidization, the Ti powder morphology was successfully changed from an irregular shape to a spherical one. Furthermore, the particle size increased (4.7 μm → 31.8 μm) due to particle coarsening. The particle size distribution was also decreased after treatment.

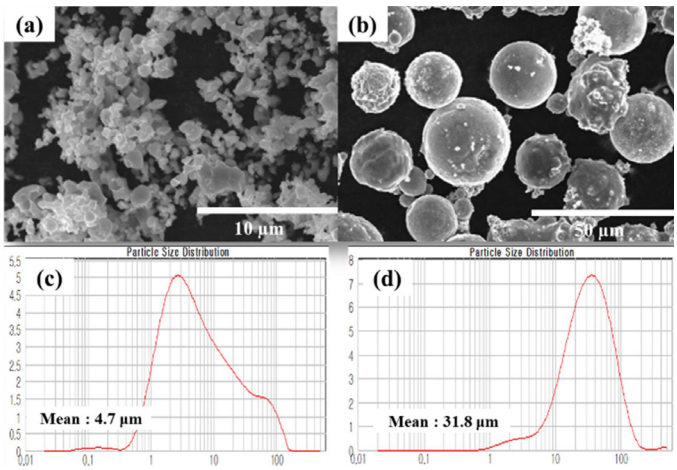

Fig. 11. FE-SEM morphology and size distribution of the Ti powders: (a,c) before and (b,d) after DC plasma treatment

4. Conclusions

In this study, single phase Ti powder was successfully fabricated by CS, and spheroidization of the resulting Ti powder was performed. Throughout the process, the possibility of obtaining Ti powder for use as raw materials for 3D printing was investigated. For the TiO_2 + αMg system studied here, a stoichiometric point of α = 2 led to the highest value of T_c (1709°C), and TiO was still present due to incomplete reduction. Mg was melted and vaporized by high exothermic heat from the reduction of titanium oxide therefore 2 mole of Mg does not perfectly used. The combustion temperature and combustion wave propagation velocity gradually decreased with increasing Mg concentration, and Ti oxide powder was successfully reduced at higher Mg concentrations. Therefore, α = 3 was chosen as the optimum conditions for the TiO_2 + αMg system, with T_c and U_c values of 1372°C and 0.26 cm/s respectively. Furthermore, this ratio also had the lowest oxygen concentration in this study (0.8 wt%). The activation energy of the TiO_2 + αMg system was calculated as 20.5 kJ/mol (using T_c and U_c). In this system, a high activation energy was not required because liquid Mg diffuses into the solid TiO_2 phase prior to reaction. Spheroidization of the as-synthesized Ti powder was carried out using DC plasma treat-

ment, which formed spherical particles with size that increased from 4.7 μm to 31.8 μm, which are more than adequate for 3D metal printing processes.

Acknowledgments

This research was supported by an internal R&D program of the Korea Institute of Industrial Technology (KITECH), funded by the Ministry of Strategy and Finance, Korea and partially supported by the technology innovation program, 10063427, Development of eco-friendly smelting technology for the production of rare metal production for lowering manufacturing costs using solid oxide membrane funded by the Ministry of Trade, Industry &Energy

REFERENCES

[1] M. Ribeiro, M. Moreira, J. Ferreira, J. Mater. Proc. Tech. **143**, 458 (2003).
[2] M. Rahman, Z. Wang, Y. Wong, JSME Int. J. Series C **49**, 11 (2006).
[3] K.H. Kramer, in: P. Lacombe, R. Tricot, G. Beranger (Eds.), Proceedings of the 6th World Conference on Titanium, Cannes, 521 (1988).
[4] Y.M. Kim, Y.B. Song, S.H. Lee, Y.S. Kwon, J. Kor. Powd. Met. Inst. **21**, 4 (2014).
[5] K.F. Leong, C.M. Cheah, C.K. Chua, Biomater. **24**, 2363 (2003).
[6] S.J. Kalita, S. Bose, H.L. Hosick, A. Bandyopadhyay, Mater. Sci. Eng. C. **23**, 611 (2003).
[7] A. Woesz, M. Rumpler, J. Stampfl, F. Varga, N. Fratzl-Zelman, P. Roschger, K. Klaushofer, P. Fratzl, Mater. Sci. Eng. C. **25**, 181 (2005).
[8] T. Boland, A. Ovsianikov, B.N. Chickov, A. Doraiswamy, R.J. Narayan, W.Y. Yeong, K.F. Leong, C.K. Chua, Adv. Mater. Process. **165**, 51 (2007).
[9] O.L.A. Harrysson, O. Cansizoglu, D.J. Marcellin-Little, D.R. Cormier, H.A. West II, Mater. Sci. Eng. C. **28**, 366 (2008).
[10] W.J. Kroll, Trans. Electrochem. Soc. **78**, 35 (1940).
[11] J. Dawes, R. Bowerman, R. Trepleton, Johnson Matthey Technol. Rev. **59**, 243 (2015).
[12] F.H. Froes, M.N. Gungor, M. Ashraf Imam, JOM **28** (2007).
[13] H.H. Nersisyan, H.I. Won, C.W. Won, J.H. Kim, J. Chem. Eng. **235**, 67 (2014).
[14] J. Gambogi, S.J. Gerdemann, DOE/ARC (1999).
[15] D.J. Fray, G.Z. Chen, T.W. Farthing, Nature **407** (6802), 361 (2000).
[16] R.O. Suzuki, K. Ono, TMS Yazawa International Symposium (2003).
[17] A.G. Merzhanov, J. Mat. Proc. Tech. **56**, 222 (1996).
[18] J.J. Moore, H.J. Feng, Prog. Mater. Sci. **39**, 275 (1995).
[19] H.H. Nersisyan, J.H. Lee, C.W. Won, Mater. Res. Bull. **38**, 1135 (2003).
[20] T.S. Azatyan, V.M. Maltsev, A.G. Merzhanov, V.A. Seieznev, Com. Explos. Shock Waves, **15**, 35 (1979).